scientific reports

Check for updates

OPEN

A novel curdlan based desiccant coated heat exchanger for efficient dehumidification

Xiaoping Lei, Wenjun Ying, Zhaoran Xue, Hua Zhang & Jiayun Wang✉

Desiccant-coated heat exchangers (DCHEs) are instrumental in dehumidification processes; however, the efficiency of existing DCHE systems is often hindered by suboptimal desiccant performance and inadequate optimization of the desiccant-heat exchanger interactions. To address these limitations, we developed a novel curdlan-based DCHE system, formulated a dynamic heat and mass transfer model in COMSOL, and assessed its dehumidification capabilities across a range of environmental conditions. Our dynamic model was experimentally validated, yielding errors of ± 10% for outlet temperature and ± 7.3% for humidity during both dehumidification and regeneration phases. Under an inlet air humidity of 80%, the system achieved a moisture removal capacity (MRC) of 11.84 g/kg and a moisture removal rate (MRR) of 79.4%. Furthermore, the coefficient of performance (COP) peaked at 2.84, with an average cooling capacity (Q) of 385.4 W at a regeneration temperature of 50 °C. This study paves the way for significantly enhancing DCHE dehumidification efficiency and presents a promising energy-saving solution for managing ambient humidity.

List of symbols

w	Moisture adsorption of desiccant, g/kg
C_p	Specific heat capacity at constant pressure, J/kg·°C
t	Time, s or min
ω	Air humidity at inlet and outlet, g/kg
T	Temperature, °C
u	Velocity vector, m/s
d_f	Fin thickness, mm
d_s	Fin spacing, mm
n	Number of flat tubes, n
d_{in}	Inner diameter of copper tube, mm
d_{out}	Outer diameter of copper tube, mm
P	Pressure, Pa
ΔF	Adsorption potential, J/mol
K_s	Adsorption rate coefficient of desiccant, 1/s
RH	Relative humidity, %
A	Cross-sectional area, m^2
k	Equation coefficient
m_a	Mass flow rate of air, kg/s
R	Universal gas constant
Q	The average cooling capacity of air

Greek symbols

η_l	Length of heat exchanger, mm
η_w	Width of heat exchanger, mm
η_h	Height of heat exchanger, mm
ρ	Density, kg/m^3
μ	Dynamic viscosity, Pa.s
λ	Thermal conductivity, J/kg·°C

Subscripts

a	Air
Al	Aluminum

Institute of Refrigeration and Cryogenics, University of Shanghai for Science and Technology, Shanghai 200093, China. ✉email: jywang@usst.edu.cn

Cu	Copper
in	Inlet
out	Outlet
de	Dehumidification
eq	Equilibrium

Abbreviations

COP_{th}	Thermal coefficient of performance
MRC	Moisture removal capacity
MRR	Moisture removal rate
DCHE	Desiccant-coated heat exchangers

Dehumidification has garnered significant attention as a key strategy for ambient humidity regulation, offering comfort to inhabitants, preventing mold proliferation, and conserving energy in industrial settings[1–5]. Air-conditioning systems, which constitute 20% of the global energy consumption, allocate 40% of their usage to humidity regulation in buildings[6,7]. Consequently, substantial improvements in energy efficiency can be achieved through effective humidity control and optimized air circulation.

Air humidity regulation is conventionally achieved through condensation or desiccant dehumidification methods. While condensation dehumidification, prevalent in traditional air conditioning systems, is energy-intensive as it involves cooling air below the dew point to extract excess moisture followed by reheating to ambient temperatures[8–11], adiabatic desiccant dehumidification stands out for its thermodynamic efficiency as an isoenthalpic process with minimal irreversible energy loss. Consequently, a desiccant-coated heat exchanger (DCHE) is favored for its low energy demand, managing both sensible and latent heat loads[12,13]. Notably, during dehumidification, the DCHE leverages cooling water flowing through its channels to dissipate adsorption heat, thereby enhancing the desiccant's moisture adsorption capabilities. Simultaneously, the heat exchanger facilitates rapid and thorough desiccant regeneration, ensuring the desiccant's continuous performance efficiency.

The dehumidification and regeneration processes of DCHEs entail the intricate coupling of heat and mass transfer between air and desiccant, as well as between desiccant and exchanger. Enhancing the efficiency of the desiccant and refining the heat exchanger structure could significantly augment the performance of existing desiccant-coated heat exchangers. Focusing on the desiccant, the majority of researchers have concentrated on identifying high-performance desiccant materials to bolster DCHE dehumidification capabilities, including metal-organic frameworks (MOFs)[14–19], zeolites[20–22], silica gel[23–25], composite desiccants[25,26], and ion exchange resin[27]. Despite advancements in desiccant research, the overall dehumidification efficiency is frequently compromised by uneven coatings when integrated with heat exchangers. Furthermore, desiccants with fixed pore volumes are prone to carryover under high-humidity conditions, leading to heat exchanger corrosion[28], diminished cycling stability[29], and reduced efficiency. In comparison, hydrogel-based desiccants, which have flexible pores[30] can absorb hundreds of times their own weight in moisture, accommodating up to 1000 g/g of liquid water, which offers a significant advantage over materials like silica gel in humidity control. Compared to some high-end Metal-Organic Frameworks (MOFs), the raw materials for hydrogels are generally more readily available and less costly. Furthermore, hydrogels can typically be prepared under mild conditions through straightforward processes and are easily shaped into various forms and sizes, suitable for diverse applications, giving them a bright future in DCHE applications[31]. Thus, we develop a novel hydrogel-based composite desiccant, Curdlan @lithium chloride(Cur@LiCl), by combining the curdlan gel and hygroscopic salt Lithium chloride(LiCl), producing a composite with a high dehumidification capacity and fast adsorption-desorption kinetics.

Researchers have employed a combination of experimental and simulation approaches to enhance the dehumidification performance of DCHEs and minimize their energy consumption. Pan et al.[32] developed a DCHE based on the desiccant material AFLi30@P and achieved a dehumidification capacity of 1.08 g/g at 27 °C/70% relative humidity (RH) and 60 °C regeneration temperature. Zheng et al.[33] developed and tested a novel superabsorbent polymer (sodium polyacrylate) and an activated carbon-based DCHE, achieving ~ 6.1 g/kg dehumidification capacity and 3.6 coefficient of performance (COP) at outdoor air conditions of 38 °C/60%RH. Vivekh et al.[34] found that by reducing the ratios of the thickness of the adsorbent layer/thickness of the fin layer (δd/δf) and H/L of a DCHE to 0.1 and 0.04, the removal of latent energy could be increased from 3.9 to 8.5 kW. Furthermore, Zu and Qin[35] analyzed the hygrothermal properties of a MOF-based humidity pump (MOF-HP) and increased the dehumidification capacity 1.59 times by optimizing its geometric design. A mathematical model to simulate heat mass exchange in a finned tube heat exchanger with desiccant was developed by Jagirdar and Lee[36], where the COP reached its maximum when the fin thickness was 0.2 mm. Nevertheless, a comprehensive analysis of the dehumidification performance of DCHEs, encompassing multidimensional factors such as high-efficiency desiccant materials and the operating conditions for dehumidification and regeneration, has been seldom undertaken in the existing literature.

While significant advancements have been made in the performance study of desiccant-coated heat exchangers (DCHEs), there is a paucity of research on dehumidification analysis using gel materials. To address this, we developed an efficient curdlan-based composite desiccant, constructed a dehumidification experimental platform to investigate its adsorption properties, and established a three-dimensional DCHE model in COMSOL based on the principles of energy, momentum, and mass conservation. Subsequently, we optimized the operational parameters for both dehumidification and regeneration stages and validated them experimentally. Unlike most current heat exchanger numerical models that rely on Darcy's law[37,38] or Convection-diffusion equation[39] to describe adsorption mechanisms, our model employs the more sophisticated LDF (linear driving force) method, which is significant for the study of heat and mass transfer in porous media. Compared to previous approaches,

Parameters	Value
Length of heat exchanger, η_l/mm	123
Width of heat exchanger, η_w/mm	112
Height of heat exchanger, η_h/mm	12
Fin thickness, d_f/mm	0.1
Fin spacing, d_s/mm	2.2
Number of flat tubes, n	12
Inner diameter of copper tube, d_{in}/mm	1.6
Outer diameter of copper tube, d_{out}/mm	2

Table 1. DCHE's dimensions.

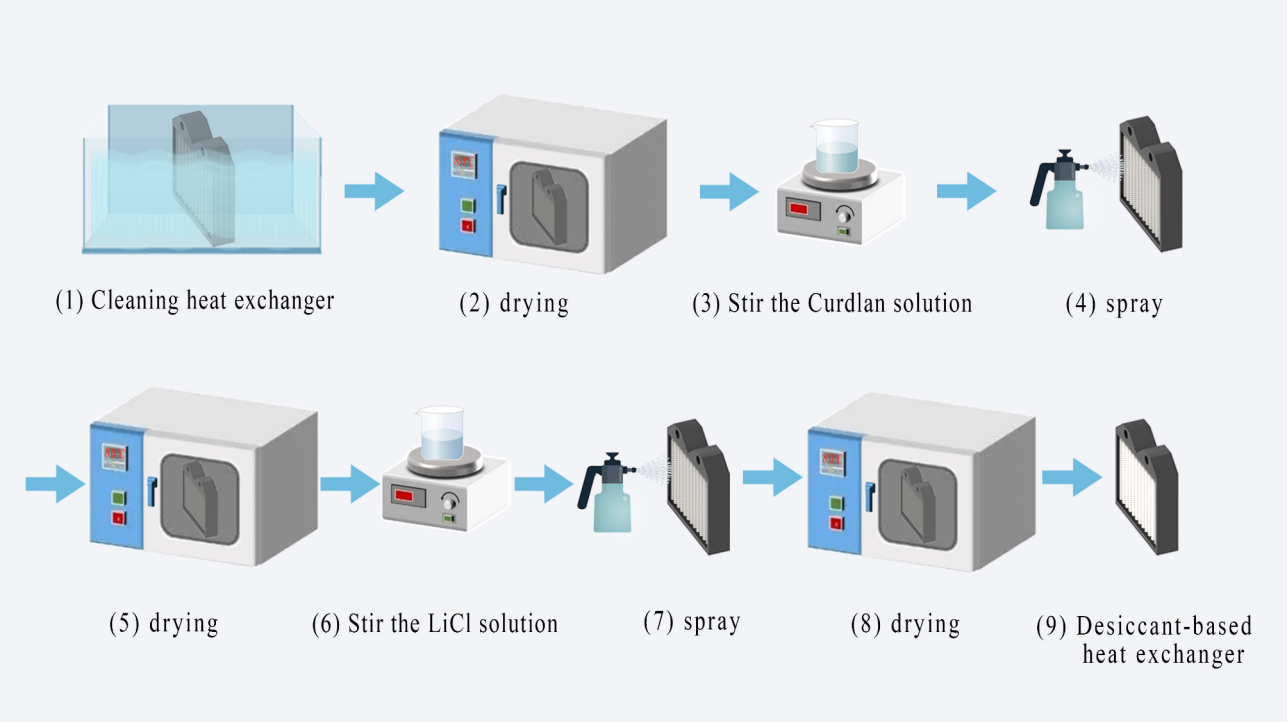

Fig. 1. Desiccant- coated heat exchanger manufacturing process. Generated using Adobe Photoshop 2021 (https://www.adobe.com/products/photoshop.html).

our method is more systematic and efficient, providing an effective avenue for predicting and optimizing DCHE performance.

Experimental methods

Preparation of Curdlan-based desiccant-coated heat exchanger

PT1120B is adopted as the microchannel heat exchanger of our DCHE system and the specific parameters are listed in Table 1.

The DCHE is manufactured by the following process: 1) immerse the microchannel heat exchanger in a sodium hydroxide solution to remove surface impurities, then dry it in the oven at 80 °C for 6 h; 2) stir the Curdlan solution with 5% concentration in a cold water bath for about 20 min to ensure it can be fully dissolved; 3) spray the Curdlan solution evenly on the desiccant heat exchanger and then dry the desiccant heat exchanger in an oven at 80 °C for 4 h; 4) spray the 15% concentration of Lithium chloride solution on the fins of the dehumidified heat exchanger, and dried it in an oven at 80 °C for 3 h. Ultimately, a uniform curdlan-based composite DCHE with a thickness of 0.2 mm is prepared through 6–8 cycles of spraying and drying, as depicted in Fig. 1. The visual comparison of the heat exchanger before and after the coating process is presented in Fig. 2.

Establishment of dehumidification systems

To measure the dynamic dehumidification performance of the desiccant-coated heat exchanger, we established an experimental system as shown in Fig. 3. In this setup, a curdlan-based desiccant heat exchanger is installed within a rectangular airflow channel. At the air inlet, a heater and humidifier are placed to achieve the required

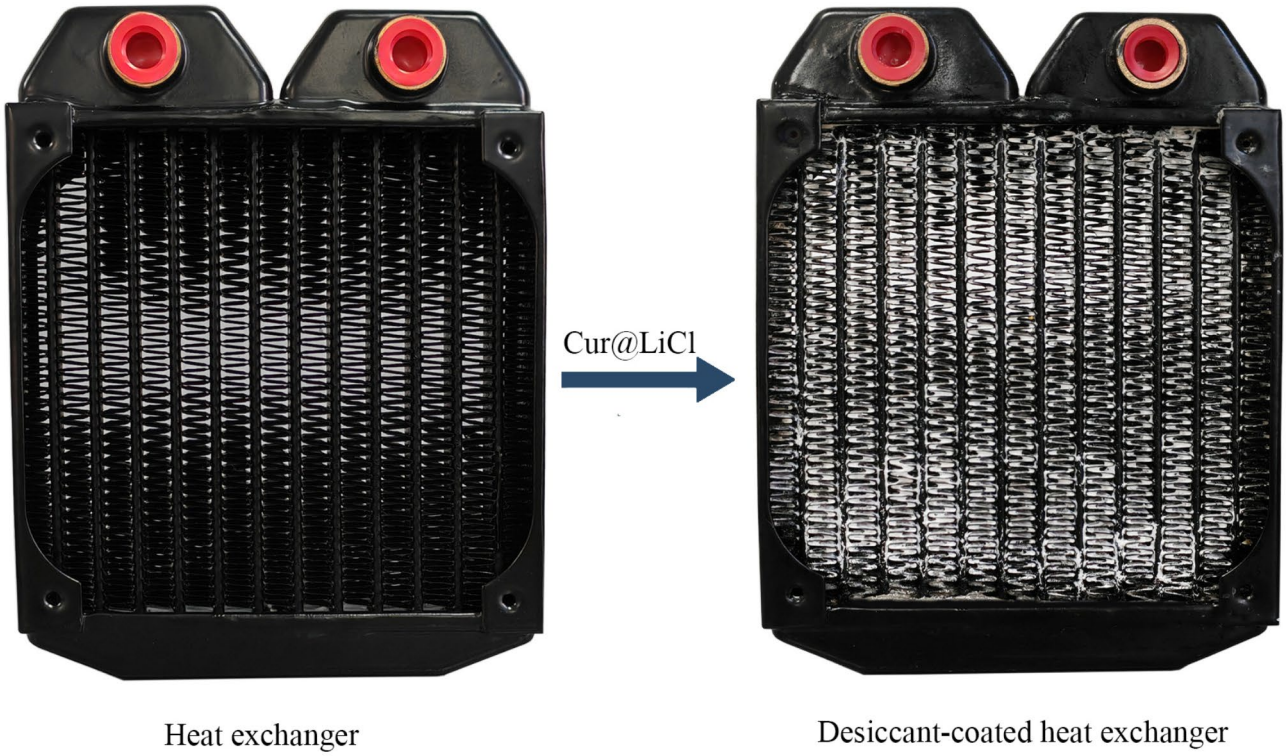

Fig. 2. Heat exchanger before and after coating.

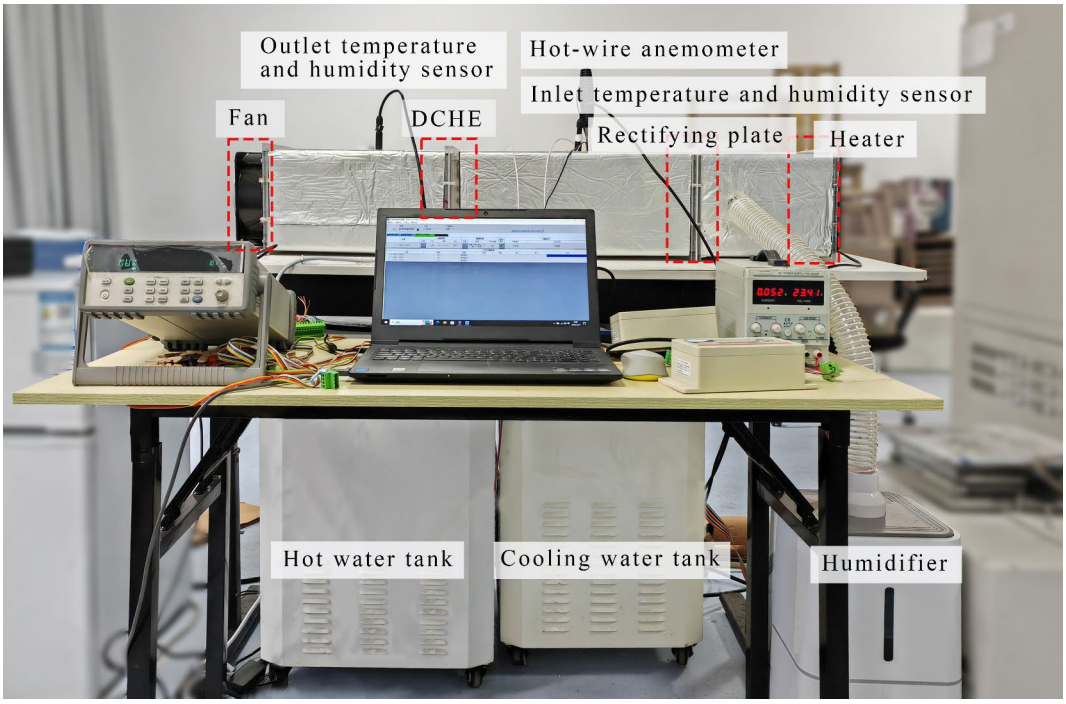

Fig. 3. Physical diagram of the experimental setup.

Materials	λ/(W/m·K))	ρ/(kg/m³)	C_p /(kJ/(kg·K)	K_s /(1/s)
Cur@LiCl	1.5	449.4	2.583	$3.48\times10^{\wedge-3}$
Air	0.0263	1.293	1.005	--

Table 2. Thermophysical properties of Cur@LiCl and air.

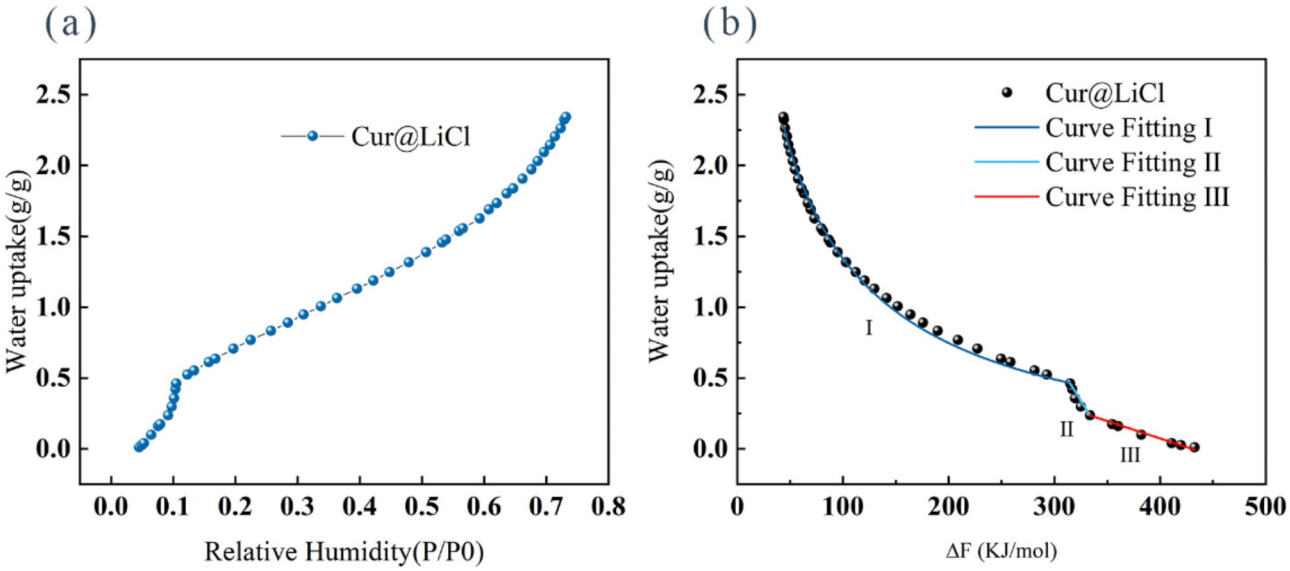

Fig. 4. (**a**) Adsorption isotherms of Cur@LiCl at 25 °C. (**b**) Adsorption equilibrium curve fitting for Cur@LiCl.

Region	ΔF(kJ/mol)	Fitting formula	R^2
I	43.65 ~ 314.97	W_{eq}=9.7575exp(-0.3547$\Delta F^{0.3737}$)	0.9987
II	314.97 ~ 333.67	W_{eq}=4.2357 – 0.012ΔF	0.9983
III	333.67 ~ 432.76	W_{eq}=1.054 – 0.0025ΔF	0.9944

Table 3. Adsorption equilibrium equation of Cur@LiCl.

temperature and humidity conditions, while a fan at the outlet regulates the flow rate of humid air entering the DCHE. Two constant-temperature water baths are used for heating or cooling the heat exchanger, ensuring efficient heat exchange.

The operating process of the DCHE consists of two phases: during the dehumidification phase, the heat generated by the adsorption process is removed by circulating cooling water from a low-temperature water bath, ensuring isothermal adsorption with a high adsorption capacity; during the regeneration phase, the DCHE is heated by a high-temperature water bath, allowing the desiccant to regenerate under heating conditions. Throughout the experiment, data were recorded using an Agilent 34,970 A data acquisition system.

The adsorption kinetics of Cur@LiCl

The material properties of Cur@LiCl desiccant and air are described in Table 2.The adsorption isotherm of Cur@LiCl at 25 °C is shown in Fig. 4(a). The adsorption capacity of Cur@LiCl is quite low when the relative humidity is below 11%, and the adsorption capacity of Cur@LiCl produces a step from 0.46 to 2.34 g/g when the relative humidity is greater than 11%, which is due to the occurrence of deliquescence of LiCl that makes the moisture adsorption increasing. The moisture adsorption of Cur@LiCl reached 2.15 g/g when the relative humidity was 70%. From the adsorption isotherm of Cur@LiCl and Eq. (14), the relationship between its water uptake and adsorption potential energy(ΔF) can be obtained as shown in Fig. 4(b). The adsorption characteristic curve of the hydrogel composite desiccant contains three parts due to the dual influence of the Curdlan and lithium chloride particles. In order to accurately characterize the equilibrium adsorption performance of Cur@LiCl, Fig. 4(b) was divided into three parts for curve fitting, and the fitting results are given in Table 3. The first part was fitted using the D-A equation (Eq. (13)), and the second and third parts were fitted linearly, respectively.

Dynamic characteristics of DCHE

Figure 5 illustrates the cyclic performance of a DCHE over four consecutive dehumidification and regeneration cycles under the standardized inlet air conditions of 25 °C/80%RH. During the dehumidification phase, the DCHE exhibits a significant reduction in the humidity ratio of the incoming air, from 15.96 to 5 g/kg, as the desiccant absorbs moisture from the wet air. However, as the desiccant approaches saturation, the humidity ratio of the air gradually increases. Upon initiating the regeneration phase by circulating hot water within the heat exchanger, the desiccant heats up, releasing a substantial amount of water vapor and causing a sharp increase in the humidity ratio at the air outlet, from 14.82 to 51.6 g/kg. As the desiccant's moisture content diminishes, the humidity ratio of the outlet air declines, demonstrating the DCHE's robust cycle stability as it alternates between dehumidification and regeneration cycles.

Numerical simulation model

Mathematical model of DCHE

A three-dimensional mathematical model of the microchannel DCHE was developed using COMSOL Multiphysics 5.6, as depicted in Fig. 6. The model encompasses various components, including copper tubes, fins, water, airflow channels, and a desiccant coating on the fins. It employs the linear driving force (LDF) model and equilibrium adsorption equations to analyze the heat and mass transfer dynamics between the adsorbent and water. The model incorporates physical fields for air and adsorbent temperature, humid air, and dilute matter transfer, with corresponding boundary conditions set for air inlets and outlets within each field.

The DCHE model incorporates non-isothermal flow, heat and moisture transfer, and multi-physics fields to achieve coupled solutions. It utilizes a mixed topology of an unstructured grid for meshing, resulting in a final

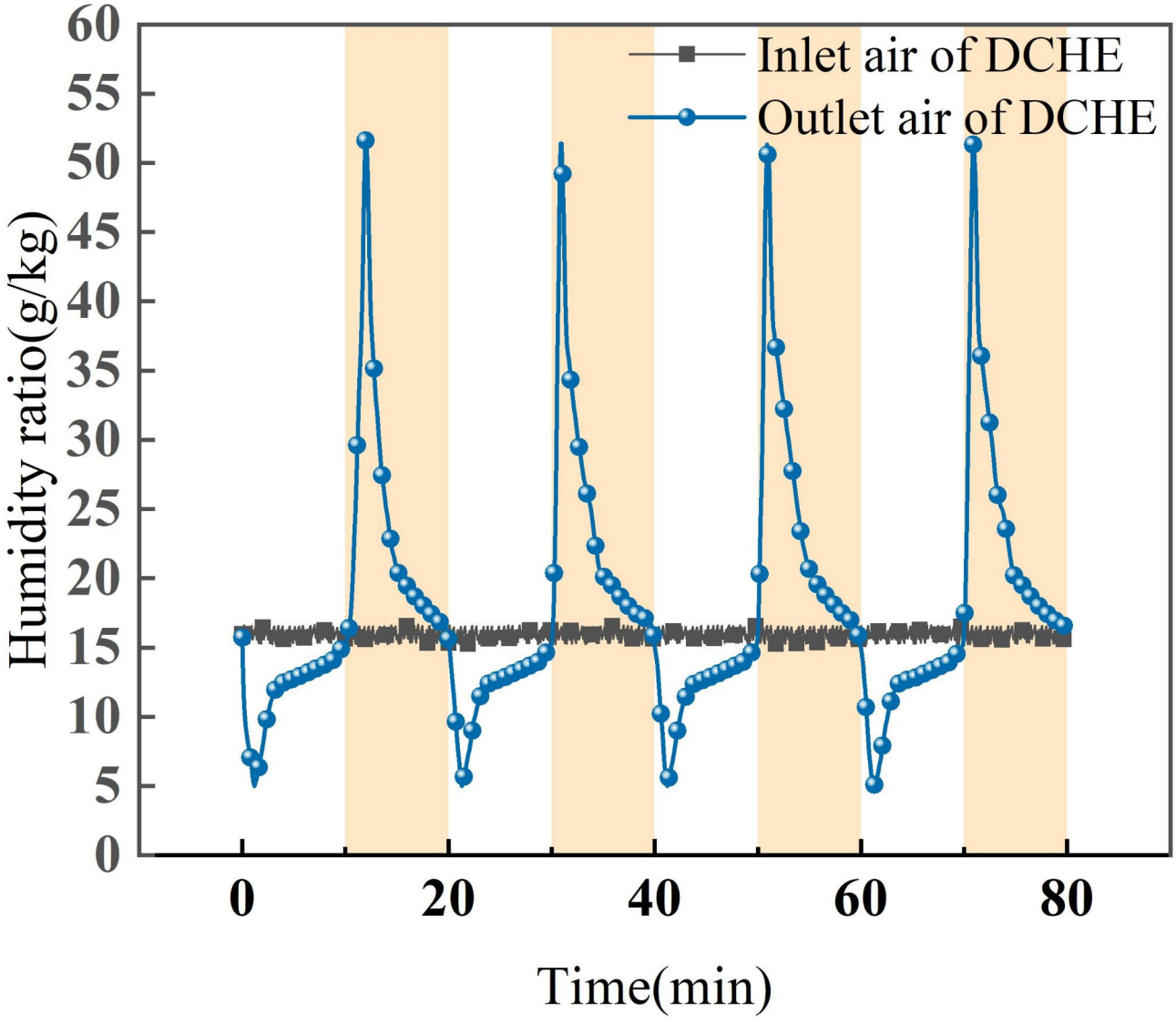

Fig. 5. Four dehumidification and regeneration cycles of the DCHE with inlet air conditions of 25 °C/80%RH (air inlet flow velocity: 0.5 m/s, cooling water: 20 °C, hot water: 80 °C).

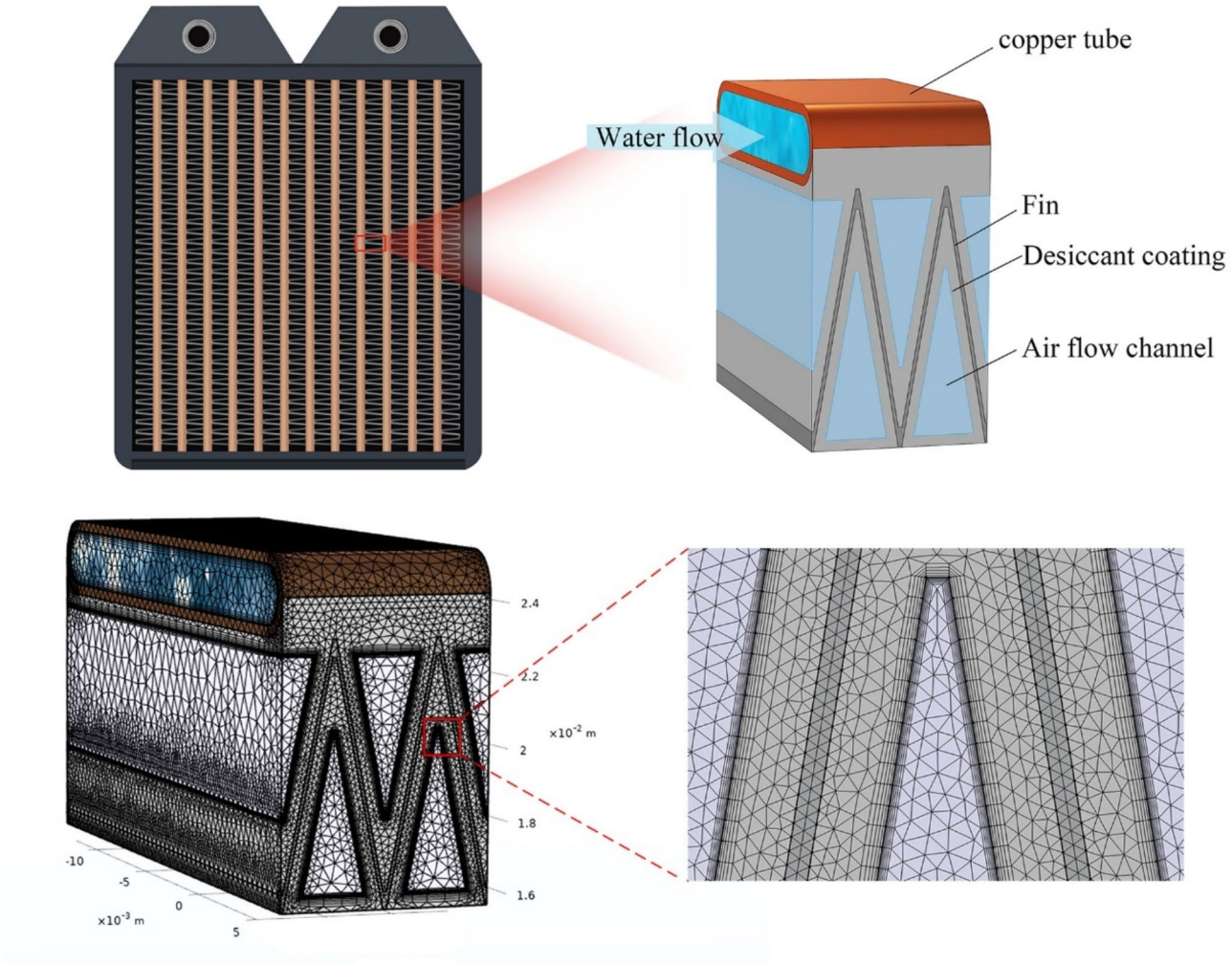

Fig. 6. DCHE numerical model and meshing. Simulation and visualization performed using COMSOL Multiphysics 5.6(https://www.comsol.com/).

grid comprising approximately 700,000 elements. The geometric model of the DCHE is discretized regionally to generate cells, and the steady-state and transient problems are subsequently solved using both COMSOL's direct and iterative solvers.

Assumptions

For the analysis, some minor factors need to be ignored and the following assumptions are made.

1. Uniform distribution of adsorbent on the fins and consistent thickness. This assumption facilitates the simplification of heat transfer and fluid dynamics calculations. In practical applications, however, the desiccant distribution may not be perfectly uniform due to manufacturing tolerances or variations in operating conditions, which could influence the performance of the heat exchanger.
2. The adsorbent, fins and copper tubes are isotropic and their density, thermal conductivity specific heat capacity, and other physical properties are constant under operating conditions. The assumption simplifies the handling of material properties, thereby making heat conduction calculations more straightforward. In practice, however, the physical properties of materials can change with variations in temperature and humidity, particularly under extreme operating conditions. Moreover, some materials may exhibit anisotropic behavior, further complicating their performance.
3. The heat of adsorption/desorption of the adsorbent is released or absorbed at the interface between the adsorbent layer and the air, the adsorbent and adsorbed adsorbent (liquid water) is in local thermal equilibrium. This assumption facilitates the simplification of thermal equilibrium calculations by treating heat transfer across the interface as instantaneous. In practice, however, heat transfer between the desiccant and the adsorbate may not occur instantaneously and could involve a time lag, potentially impacting the establishment of thermal equilibrium.
4. The heat loss at the end of the fins and the end of the copper tube and the effect of radiation are neglected, ignoring the contact thermal resistance of fins and adsorbents. Ignoring these factors facilitates the sim-

plification of heat loss calculations. In practical applications, however, contact thermal resistance and heat losses are unavoidable and can significantly affect the efficiency of the heat exchanger. Additionally, radiation becomes an important mode of heat transfer, particularly at high temperatures.

5. The air flow through the fins and the heat transfer fluid are in a fully developed laminar flow state, and their flow state does not change with time. This assumption facilitates the prediction and control of flow conditions, as fully developed laminar flow is highly predictable. In practical applications, however, the flow state may be affected by multiple factors, such as variations in flow velocity and system vibrations, leading to potential changes in the flow state over time.

Governing equations

Based on the above assumptions, the control equations in different computational domains of the DCHE 3D model are established.

Air domain

fluid flow, heat and mass transfer and diffusion due to concentration differences are involved processes, the corresponding control equations are as follows:

$$\rho_a(\nabla u_a) = 0 \tag{1}$$

$$\rho_a \left[\frac{\partial u_a}{\partial t} + (u_a \cdot \nabla)\, u_a\right] = -\nabla P_a + \mu_a \nabla u_a \tag{2}$$

$$\rho_a C_{p,a} \left(\frac{\partial T_a}{\partial t} + u_a \cdot \nabla T_a\right) + \nabla \cdot (-\lambda_a \nabla T_a) = 0 \tag{3}$$

$$\frac{\partial \omega_a}{\partial t} + \nabla \cdot (-D_a \nabla \omega_a) + u_a \cdot \nabla \omega_a = 0 \tag{4}$$

Adsorbent domain

There is energy exchange and substance exchange and diffusion of adsorbents,

$$(\rho C_p)_e \frac{\partial T_s}{\partial t} + \nabla\,(-\lambda_s \nabla T_s) = 0 \tag{5}$$

$$\frac{\partial w}{\partial t} + \nabla \cdot (-D_s \nabla w) = 0 \tag{6}$$

Fin and copper tube domain

There is no material transfer in the fins and copper tubes, only energy changes,

$$\rho_{Al} C_{p,Al} \frac{\partial T_{Al}}{\partial t} + \nabla \cdot (-\lambda_{Al} \nabla T_{Al}) = 0 \tag{7}$$

$$\rho_{Cu} C_{p,Cu} \frac{\partial T_{Cu}}{\partial t} + \nabla \cdot (-\lambda_{Cu} \nabla T_{Cu}) = 0 \tag{8}$$

Where ρ_{Al} (kg/m^3) and ρ_{Cu} (kg/m^3) are the density of aluminum fin and copper tube, kg/m^3, λ_{Al} (W/m·°C) and λ_{Cu} (W/m·°C) are the thermal conductivity of aluminum fin and copper tube, $C_{p,Al}$ (J/kg·°C) and $C_{p,Cu}$ (J/kg·°C) are the constant pressure specific heat of aluminum fin and copper tube, T_{Al} (°C) and T_{Cu} (°C) are the temperature of aluminum fin and copper tube, respectively.

Fluid domain

In the heat transfer fluid domain, it is mainly concerned with the flow of the fluid and the energy changes,

$$\rho_l\,(\nabla u_l) = 0 \tag{9}$$

$$\rho_l \left[\frac{\partial u_l}{\partial t} + (u_l \cdot \nabla)\, u_l\right] = -\nabla P_l + \mu_l \nabla^2 u_l \tag{10}$$

$$\rho_l C_{p,l} \left(\frac{\partial T_l}{\partial t} + u_l \cdot \nabla T_l\right) + \nabla \cdot (-\lambda_l \nabla T_l) = 0 \tag{11}$$

where u_l (m/s) is the velocity of the heat transfer fluid, μ_l (Pa·s) is the dynamic viscosity of the heat transfer fluid, and T_l (°C) is the temperature of the heat transfer fluid.

Auxiliary equations

The mass transfer process between the air domain and the contact surface of the adsorbent domain can be described by the linear driving force (LDF) model and the equilibrium adsorption equation.The LDF model of adsorption kinetics is often used successfully for the analysis of adsorption kinetic data and adsorption process design because of its simple form and the defined physical meaning of the parameters in the model, which can be represented as

$$\frac{dw_t}{dt} = K_s\left(w_{eq} - w_t\right) \tag{12}$$

Where w_t (g/kg) is the instantaneous moisture adsorption amount of desiccant and w_{eq} (g/kg) is the equilibrium moisture adsorption amount of desiccant.

$$w_{eq} = x_0 \exp(-k\Delta F^n) \tag{13}$$

x_0, k, n are the equation coefficients and ΔF is the adsorption potential, which is a function of the relative pressure and temperature of the water vapor, as displayed in Table 3.

$$\Delta F = -RT \ln \frac{P}{P_{sat}} \tag{14}$$

where R (J/(mol·°C)) indicates the gas constant, T (°C) indicates the adsorbent temperature, P (Pa) indicates the partial pressure of water vapor at the time of adsorption, and P_{sat} (Pa) indicates the saturated vapor pressure of water vapor.

$$P_{sat} = \exp\left(23.196 - \frac{3816.44}{T - 46.13}\right) \tag{15}$$

Uncertainty analysis

Due to factors such as inaccurate equipment calibration, environmental condition variations, and improper equipment usage, the data acquired from experimental measurements of temperature, pressure, flow rate, and relative humidity may be subject to errors. Table 4 provides an overview of the measurement uncertainties associated with the experimental apparatus, encompassing the temperature and humidity sensor, hot-wire anemometer, pressure gauge, and flow meter. In this study, to perform an uncertainty analysis[40], the root mean square method proposed by Holman was employed. The following presents the correlations used for error analysis:

$$\delta Er = \left[\left(\frac{\partial f}{\partial z_1}\right)^2 (\delta Z_1)^2 + \left(\frac{\partial f}{\partial z_2}\right)^2 (\delta Z_2)^2 + \ldots + \left(\frac{\partial f}{\partial z_n}\right)^2 (\delta Z_n)^2\right]^{1/2} \tag{16}$$

$$\frac{\delta Er}{Er} = \left[\left(\frac{\partial f}{\partial Z_1}\right)^2 \left(\frac{\delta Z_1}{Er}\right)^2 + \left(\frac{\partial f}{\partial Z_2}\right)^2 \left(\frac{\delta Z_2}{Er}\right)^2 + \ldots + \left(\frac{\partial f}{\partial Z_n}\right)^2 \left(\frac{\delta Z_n}{Er}\right)^2\right]^{1/2} \tag{17}$$

Where, f is the function of an independent variable and the variables of functions are Z_1,Z_2 etc. The complete errors associated with the variables are δZ_1, δZ_2 etc. while the relative error is $\frac{\delta Er}{Er}$. Through this computation, the observed average relative uncertainty in the system efficiency is 2.37%.

Performance evaluation factors of of DCHE

The Moisture removal capacity (MRC) is used to characterize the average dehumidification performance of the DCHE in a fixed dehumidification time. The Moisture removal capacity is expressed as

$$MRC = \frac{\int_0^{t_{de}} (\omega_{a,in} - \omega_{a,out}) dt_{de}}{t_{de}} \tag{18}$$

Where t_{de} (s) is dehumidification time; $\omega_{a,in}$ (g/kg) is the humidity ratio of the air inlet; $\omega_{a,out}$ (g/kg) is the humidity ratio of the air outlet.

Moisture removal rate (MRR) indicates the rate of change of humidity ratio after the air flow through the DCHE, in general, the higher the MRR means that the dehumidification performance of the DCHE is better.

$$MRR = \frac{MRC}{\omega_{a,in}} \tag{19}$$

The average cooling capacity of air (Q) is calculated using Eq. (20).

Experimental apparatus	Uncertainty [%]
Temperature sensor	± 0.51
Humidity sensor	± 0.51
Hot-wire anemometer	± 2.14
Pressure gauge	± 3.57
Flow meter	± 1.32

Table 4. Measurement uncertainty of the experimental apparatus.

$$Q = m_a(h_{a,in} - h_{a,out}) \tag{20}$$

where $h_{a,in}$(kJ/kg) and $h_{a,out}$(kJ/kg) represent the specific enthalpy of process air at inlet and outlet, respectively, during the dehumidification process; m_a (kg/s) is the mass flow rate of air. The energy use efficiency of the entire dehumidification system can be described by the thermal coefficient of performance (COP_{th}).

$$COP_{th} = \frac{Q}{m_l C_{p,l}(T_{l,in} - T_{l,out})} \tag{21}$$

In which m_l (kg/s) is the mass flow rate of water, $C_{p,l}$ (kJ/kg °C) is the specific heat capacity of water at constant pressure, $T_{l,in}$ (°C) and $T_{l,out}$ (°C) are the hot water temperature of the DCHE copper pipe in and out of the regeneration process, respectively.

Experimental results and validation

Validation with baseline conditions

The numerical model was initially validated against experimental data obtained from the DCHE experimental setup under the condition of 25 °C/80%RH inlet air. The parameters for the mathematical simulation were aligned with those of the experiment, with dehumidification and regeneration times set to 1200s. As indicated in Fig. 7(a), during the dehumidification and regeneration phases, the normalised root mean square error (NRMSE) of the outlet humidity of the numerical simulation and of the experiment is within 7.3%. In the dehumidification stage, the numerical simulation data are smaller than in the experimental data because in the actual process, there is thermal resistance of the adsorbent and fins, and the average cooling capacity of air between the system and the environment. Figure 7(b) compares the transient response of the air outlet temperature $T_{a,out}$ throughout the process in the experiment and simulation, with the maximum error between the two being within ± 10%, which is due to ambient heat loss during the experiment.

Validation of dehumidification performance at different cooling water temperatures

Figure 8 presents a comparative analysis of the transient responses of the air outlet humidity ratio and air outlet temperature between the experimental data and simulation results. With an increase in the cooling water temperature from 23 to 29 °C, the NRMSE for the outlet humidity ratio is recorded at 7.8% for the experiment and 11% for the simulation, while the maximum error for the air outlet temperature ($T_{a,out}$) remains within ± 5% for both scenarios. The slight rise in air outlet temperature corresponds to the increase in cooling water temperature, as the desiccant releases heat during the moisture adsorption process in dehumidification; consequently, cooler water is more effective at removing heat, thus enhancing the dehumidification effect. The numerical simulation model demonstrates acceptable simulation errors and high reliability, validating its use for predicting the dynamic dehumidification performance of a DCHE in various simulations.

Parametric studies

The experimental parameters, including air inlet humidity, temperature, and velocity, as well as cooling and hot water temperatures, are detailed in Table 5. Figure 9(a) presents the relative humidity distribution within the

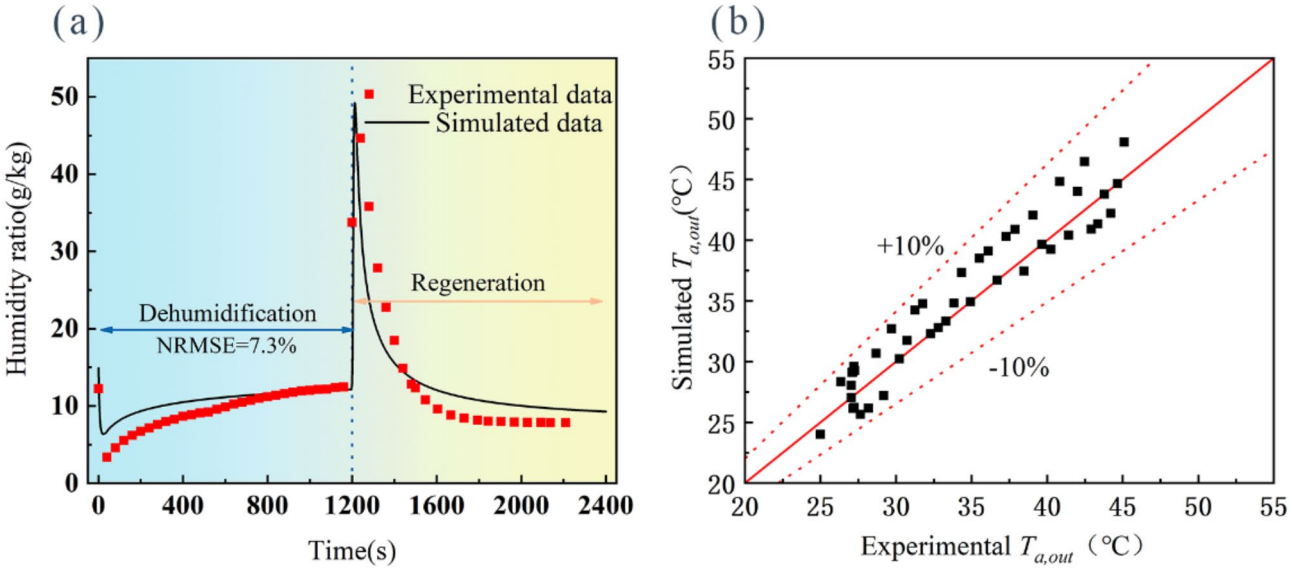

Fig. 7. Comparisons of (**a**) the outlet air humidity ratios of the simulation and experimental results at a cycle time of 1200s, (**b**) accuracy of the air outlet temperature in the numerical simulation and experiment. (Inlet air 25 °C/80%RH, air inlet flow velocity: 1 m/s, cooling water: 25 °C, hot water: 80 °C)

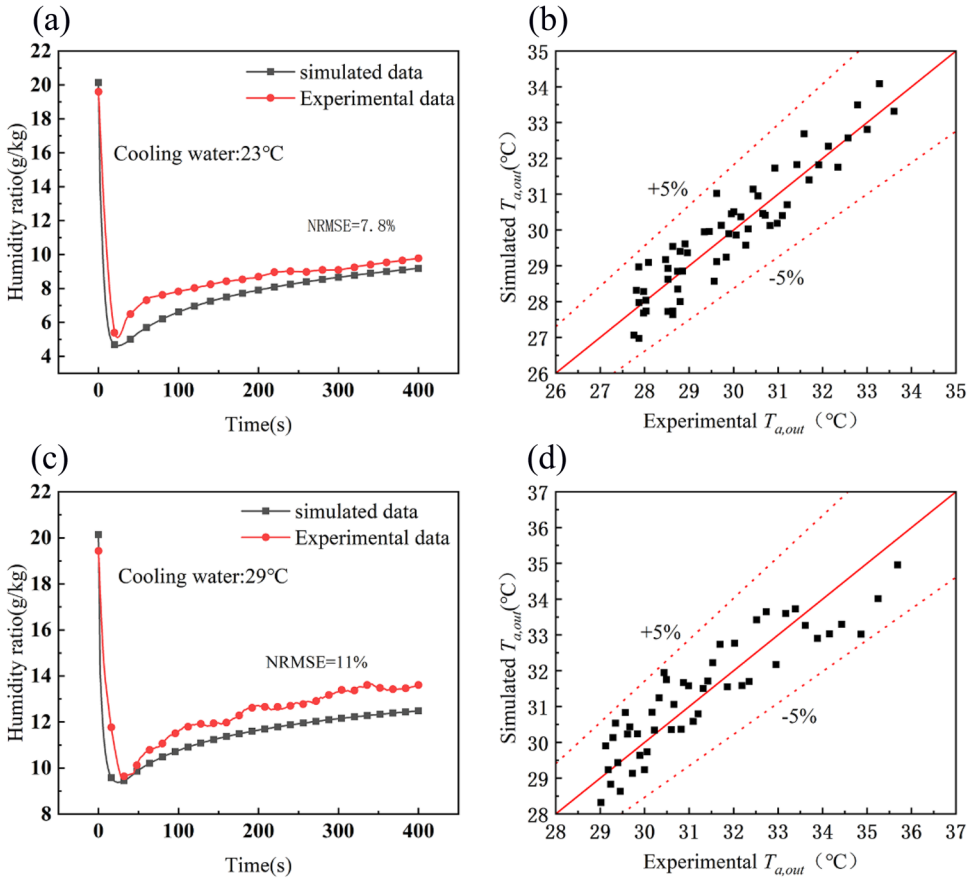

Fig. 8. Comparisons of simulation and experimental results: (**a**) humidity ratio of the DCHE outlet air when the cooling water is 23 °C, (**b**) outlet air temperature when the cooling water is 23 °C, (**c**) humidity ratio of the DCHE outlet air when the cooling water is 29 °C, (**d**) outlet air temperature when the cooling water is 29 °C.

Parameters	Variation range
Cooling water temperature /°C	20, 23, 26, 29
Air inlet humidity /%	50, 60, 70, 80
Inlet air temperature/°C	19, 22, 25, 28
Inlet air velocity /m/s	1, 1.5, 2, 2.5
Hot water temperature/°C	50, 60, 70, 80

Table 5. Variable conditions for DCHE performance testing.

air channel at a 400-second simulation time point during the dehumidification phase, while Fig. 9(b) displays the corresponding temperature distribution. Initially, the entrance region exhibits high relative humidity, which subsequently decreases as the moist air traverses the DCHE. The desiccant coating on the fins progressively adsorbs moisture, leading to a reduction in relative humidity at the outlet. Concurrently, the continuous release of adsorption heat during the desiccant's adsorption process results in a higher air outlet temperature compared to the inlet.

Dehumidification stage

Effect of cooling water temperature

Figure 10(a) illustrates that the air outlet humidity ratio escalates with the increase in cooling water temperature, achieving optimal dehumidification at a temperature of 20 °C. Figure 10(b) indicates that when the cooling water temperature increases from 20 to 29 °C, the moisture removal capacity (MRC) decreases from 15.81 to 8.7 g/kg and the moisture removal rate (MRR) decreases from 78.5 to 43.2%. Utilizing lower temperatures for cooling water not only augments the adsorption heat removal, thereby enhancing the dehumidification efficacy of the adsorbent in a process akin to isothermal dehumidification, but also facilitates the cooling of moist air below the dew point, simplifying the detachment of condensate from the air.

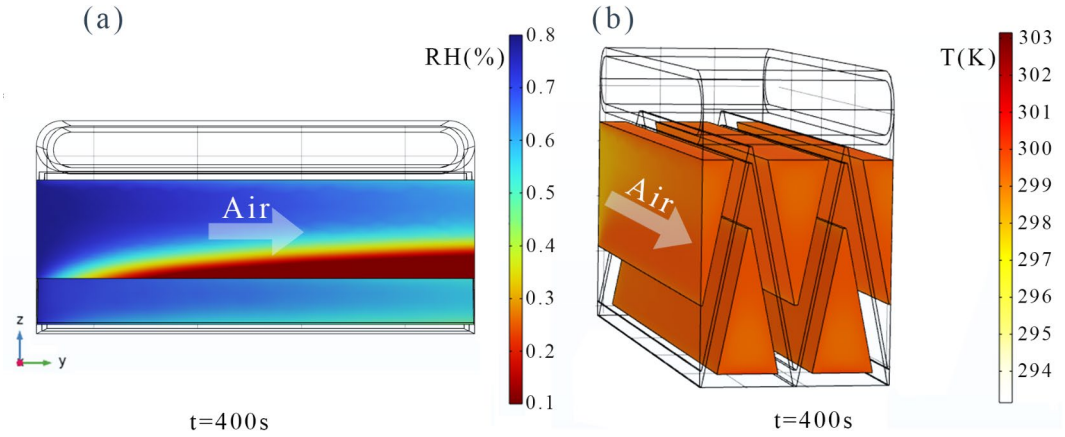

Fig. 9. The relative humidity distribution and temperature distribution of the air flow channel in the DCHE numerical model when time = 400s. (Inlet air condition: 25 °C/80%RH, cooling water temperature: 25 °C). Simulation and visualization performed using COMSOL Multiphysics 5.6 (https://www.comsol.com/).

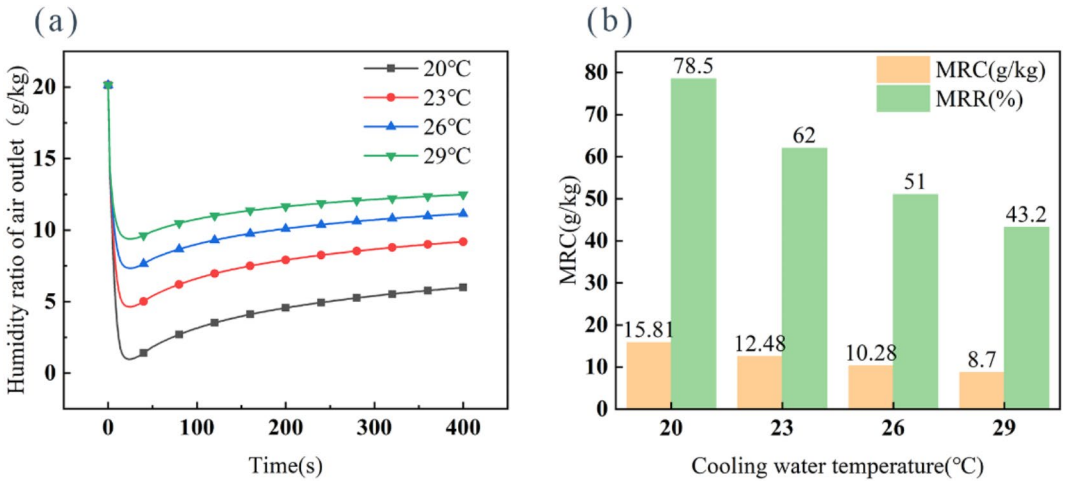

Fig. 10. (**a**) Humidity ratios of the air outlet of the DCHE in the dehumidification stage under different cooling water temperatures; (**b**) MRR and MRC of the DCHE for varying air flow channel lengths during dehumidification. (Inlet air condition: 30 °C/60%RH)

Effect of air inlet humidity

The impact of air inlet relative humidity on the adsorptive capacity of the desiccant coating within the DCHE is pronounced, as depicted in Fig. 11(a), where the disparity between the minimum outlet air humidity ratio and the inlet value expands from 4.13 to 9.56 g/kg with an increase in inlet air relative humidity from 50 to 80%. Figure 11(b) further illustrates that both MRC and MRR escalate with higher inlet humidity levels. Specifically, as the inlet air relative humidity rises from 50 to 80%, the MRC climbs from 5.86 to 11.84 g/kg, and the MRR soars from 39.3 to 79.4%. Collectively, these findings underscore that elevated inlet air humidity ratios bolster the dehumidification efficacy of the adsorbent coating, optimizing the DCHE's performance in conditions of high humidity.

Effect of inlet air temperature

As the temperature of the inlet air increases, the humidity ratio of the dehumidified heat exchanger air outlet also increases. Figure 12(a) shows that when the inlet air temperature is 19 °C, the humidity ratio of the DCHE outlet air is minimized, indicating that most of the moisture in the wet air is removed by adsorption. When the inlet air temperature is 28 °C, the humidity ratio of the air outlet is higher, and the moisture removal effect is not good. The lower the inlet air temperature, the better the dehumidification effect. Figure 12(b) shows that the MRC decreases from 11.14 to 2.66 g/kg and the MRR decreases from 74.68 to 17.8% when the air inlet temperature increases from 19 to 28 °C. The maximum values of MRR and MRC are achieved at an air inlet temperature of 19 °C. Due to the direct contact between the inlet air and the adsorbent, higher inlet air temperatures lead to increased adsorbent temperatures, which is detrimental to the removal of heat generated by the adsorption process, resulting in reduced adsorption and dehumidification capabilities.

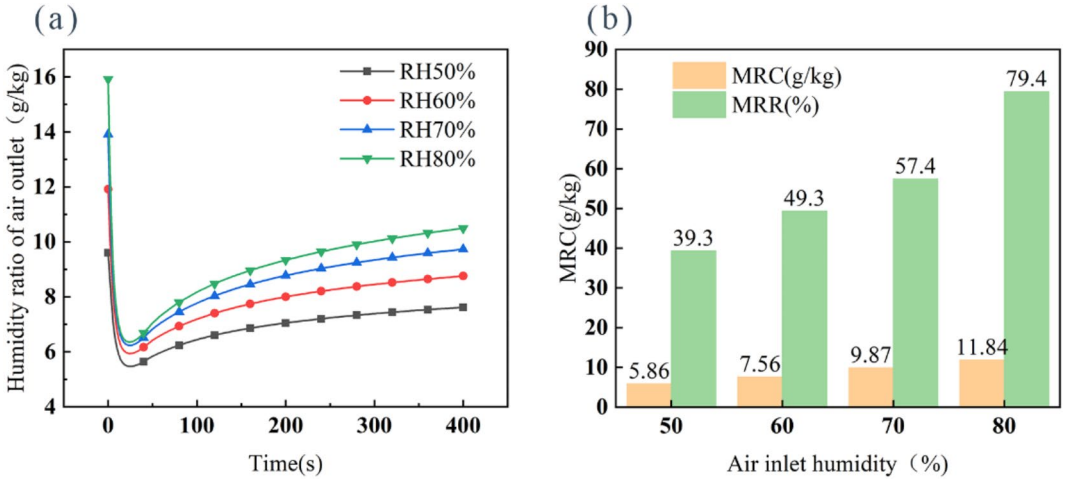

Fig. 11. (**a**) Humidity ratio of the air outlet of the DCHE in the dehumidification stage under different levels of air inlet relative humidity, (**b**) MRR and MRC of the DCHE under variations in air inlet relative humidity. (Inlet air condition: 25 °C, cooling water temperature: 25 °C)

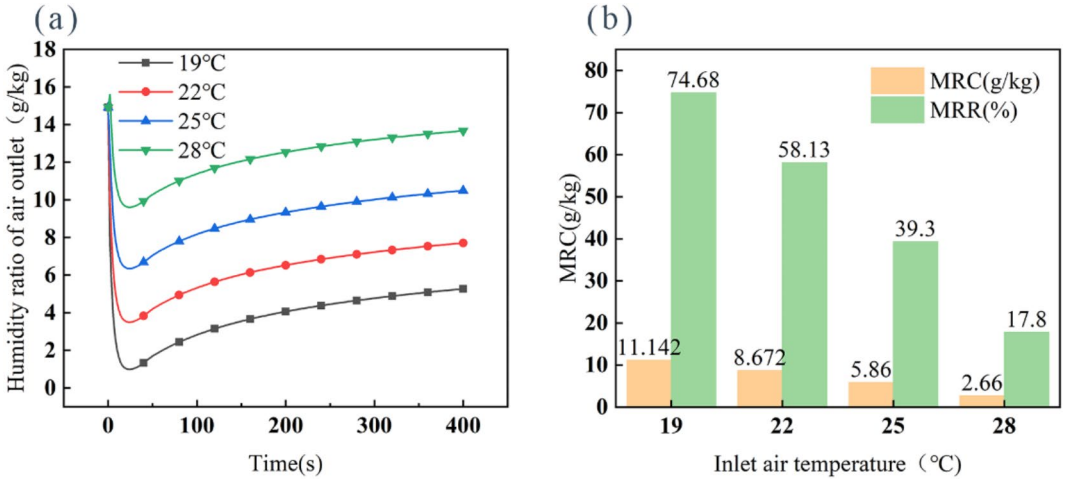

Fig. 12. (**a**) Humidity ratio of the air outlet of the DCHE at the dehumidification stage under different inlet air temperatures, (**b**) MRR and MRC of the DCHE under variations in inlet air temperature. (Inlet air condition: 80%RH, cooling water temperature: 18 °C)

Effect of inlet air velocity

Figure 13(a) illustrates that the humidity ratio at the DCHE's air outlet progressively rises with increasing inlet air velocity, reaching its minimum at a velocity of 1 m/s, indicating optimal moisture adsorption by the DCHE under this condition and high dehumidification efficiency. Conversely, at an air flow velocity of 2.5 m/s, the DCHE fails to fully adsorb the moisture from the wet air, resulting in a higher outlet humidity ratio and a diminished dehumidification effect. As shown in Fig. 13(b), augmenting the air inlet flow rate from 1 to 2.5 m/s leads to a decrease in MRC from 5.86 to 2.03 g/kg and a decline in MRR from 39 to 13.6%. This reduction in dehumidification performance is attributed to the shortened contact time between the adsorbent coating and the air at higher flow rates, which in turn diminishes the heat and mass transfer efficacy and the overall dehumidification capability of the DCHE.

Desorption stage

Effect of hot water temperature

The humidity ratio at the DCHE outlet increases as the regeneration temperature increases, as can be seen in Fig. 14(a). This is due to the fact that the higher the temperature, the stronger the desorption of moisture. The humidity ratio of the air outlet at a regeneration temperature of 80 °C is 5.51 g/kg more than that at a regeneration temperature of 50 °C. Figure 14(b) reveals that when the regeneration temperature is increased from 50 to 80 °C, the average cooling capacity(Q) of the air decreases from 385.4 to 38.17 W and the COP decreases from 2.84 to 0.28. Optimal regeneration performance of the DCHE is achieved at a hot water temperature of 50°C, where

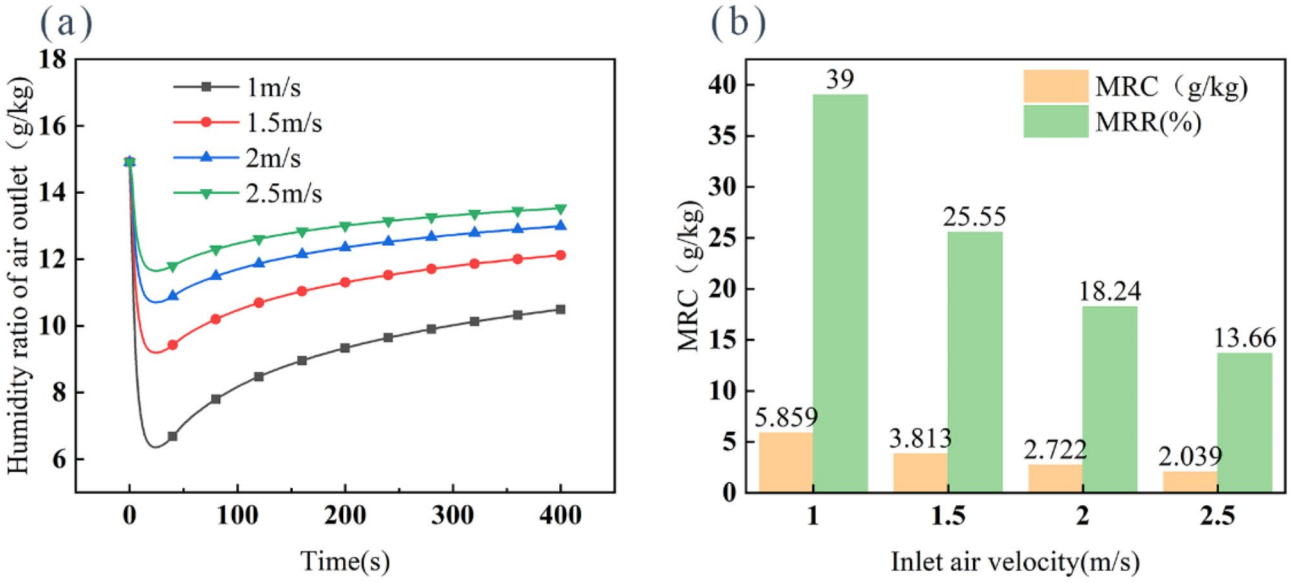

Fig. 13. (**a**) Humidity ratio of the air outlet of the DCHE in the dehumidification stage under different inlet air velocities, (**b**) MRR and MRC of the DCHE under variations in inlet air velocity. (Inlet air condition: 25 °C/80%RH, cooling water temperature: 25 °C)

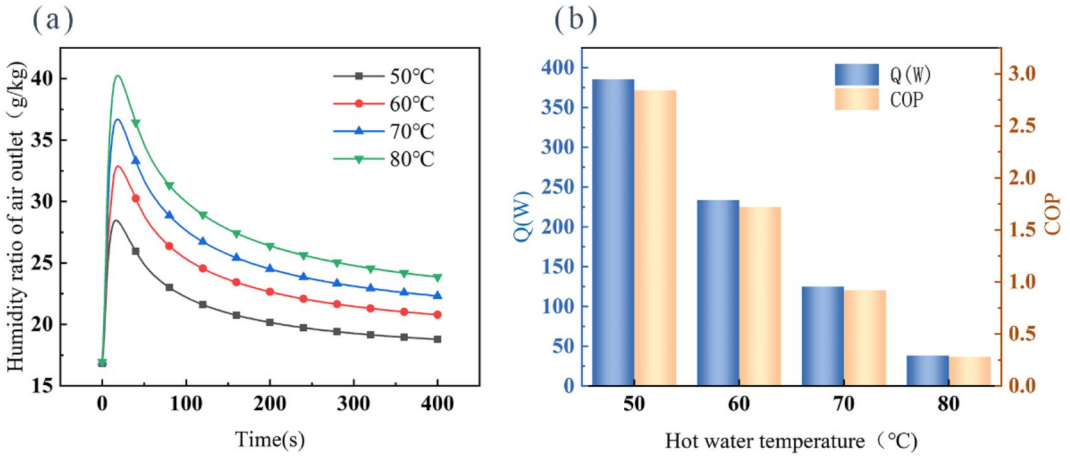

Fig. 14. (**a**) Humidity ratio of the air outlet of the DCHE in the desorption phase under different hot water temperatures, (**b**) COP and Q of the DCHE under variations in hot water temperature. (Inlet air condition: 25 °C/80%RH, cooling water temperature: 25 °C)

lower temperatures necessitate less heat for the desorption process and result in reduced ambient heat loss, thereby demonstrating the system's potential to harness low-grade heat sources for efficient moisture desorption and regeneration, enhancing the overall energy efficiency of the DCHE.

Effect of air inlet humidity

Figure 15(a) shows that the humidity ratio of the outlet air from the DCHE rises with the increase in inlet air relative humidity, with the outlet air humidity ratio at 80% inlet air relative humidity being 7.27 g/kg higher than at 50% inlet air relative humidity. The ability to desorb moisture from the wet air is highest when the inlet air is at 50% humidity. Increasing the inlet air humidity makes it more difficult to desorb moisture from the desiccant, and increasing the inlet humidity increases the energy required for dehumidification and regeneration; thus, both the average cooling capacity of air and the COP decrease, as can be seen in Fig. 15(b). When the air inlet humidity increases from 50 to 80%, the average cooling capacity of air decreases from 366.7 to 150 W and the COP decreases from 2.69 to 1.103. Thus, decreasing the inlet air humidity increases the energy efficiency of the desorption process of the DCHE system.

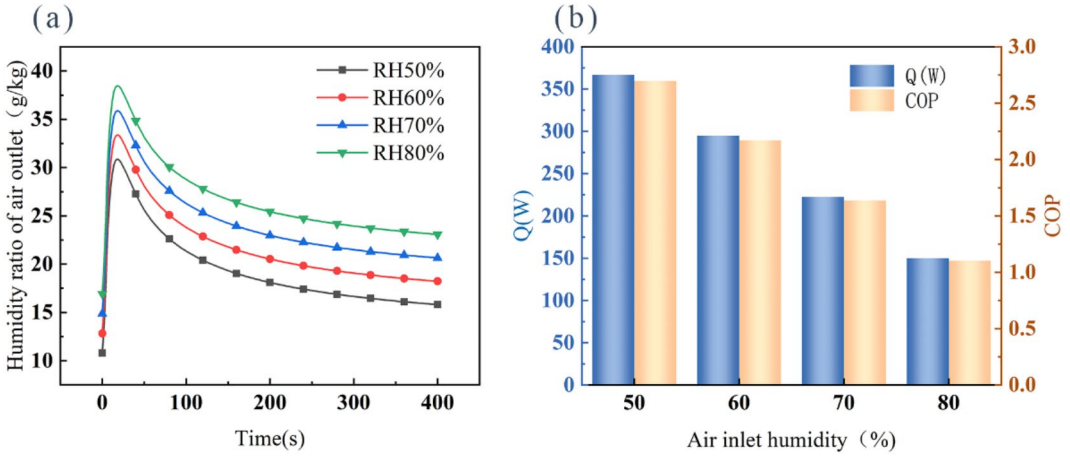

Fig. 15. (**a**) Humidity ratio of the air outlet of the DCHE in the desorption phase under different levels of air inlet relative humidity, (**b**) COP and Q of the DCHE under variations in air inlet relative humidity. (Inlet air condition: 25 °C/80%RH, cooling water temperature: 25 °C, hot water temperature: 75 °C)

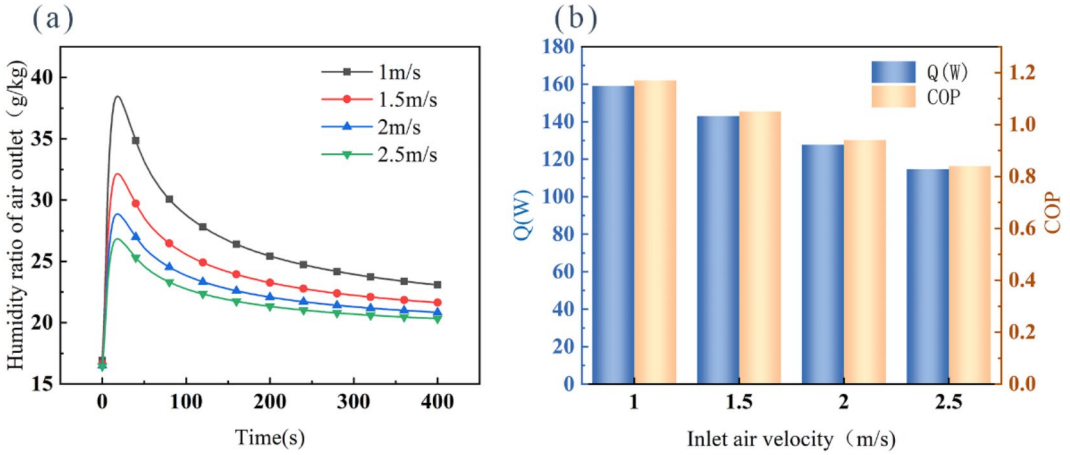

Fig. 16. (**a**) Humidity ratio of the air outlet of the DCHE in the desorption phase under different inlet air velocities, (**b**) COP and Q of the DCHE under variations in inlet air velocity. (Inlet air condition: 25 °C/80%RH, cooling water temperature: 25 °C, hot water temperature: 75 °C)

Effect of inlet air velocity

Figure 16(a) illustrates a diminishing difference in outlet humidity ratio between the initial and equilibrium stages of the desorption process as the inlet air velocity increases. Specifically, when the inlet air velocity rises from 1 to 2.5 m/s, the humidity ratio regenerated by desorption from wet air is reduced from 15.47 to 6.51 g/kg. Figure 16(b) further reveals that an escalation in airflow velocity corresponds with a decline in both the average cooling capacity of the air and the COP, with peak values of 159.1 W for cooling capacity and 1.17 for COP recorded at an air flow rate of 1 m/s. Consequently, augmenting the inlet air velocity results in heightened energy consumption for the DCHE and a diminished capacity for moisture regeneration.

Practical implications and applications

The equipment examined in this study demonstrates excellent environmental adaptability by adjusting its performance across varying conditions, including different cooling water temperatures and inlet air humidity levels. This flexibility is especially significant for applications across diverse climatic regions, which enhances the device's versatility and market acceptance.

In Heating, Ventilation, and Air Conditioning systems(HVAC) systems, effective humidity control is critical for improving indoor comfort and air quality. By integrating DCHE devices into HVAC systems, more efficient dehumidification can be achieved, along with reduced energy consumption. In industrial applications, such as food processing, pharmaceutical manufacturing, and electronics production, the high efficiency and stability of DCHE devices position them as strong alternatives to traditional dehumidification methods. Optimizing parameters such as hot water temperature, inlet air humidity, and flow rate during the regeneration phase further reduces energy requirements, leading to lower production costs and improved energy efficiency.

Conclusions

This study presents the uniform fabrication of curdlan-based desiccant-coated heat exchanger and the development of a numerical model, which has been rigorously validated through both simulation and experimental methods. The DCHE device demonstrated high efficiency and stability, sustaining effective adsorption-regeneration cycles under environmental conditions of 25ºC/80%RH, with an impressive instantaneous dehumidification capacity of 10.96 g/kg, highlighting its broad applicability. Drawing from the findings of this research, we have arrived at the following conclusions.

(1) In this study, we diverged from conventional models by integrating the LDF model to provide a more comprehensive description of the adsorption kinetics of Cur@LiCl. Additionally, we employed an optimized desiccant coating process, resulting in a uniform coating on the novel heat exchanger that significantly reduced the discrepancy between our model predictions and experimental data under reference conditions to a mere 7.3%.
(2) During the dehumidification process, the effectiveness is significantly enhanced by reducing the temperature of the cooling water. Specifically, at a cooling water temperature of 20 °C, the MRC reaches 15.81 g/kg and the MRR achieves 78.5%. Furthermore, higher inlet air humidity enhances the dehumidification performance of the DCHE. For instance, when the inlet air humidity is 80%, the MRC reaches 11.84 g/kg and the MRR reaches 79.4%. The lower air inlet velocity can improve the dehumidification effect of the system, when the air inlet velocity is 1 m/s, the MRC is 5.86 g/kg, and the MRR reaches 39%.
(3) During the regeneration phase, when the hot water temperature is 50 °C, the average cooling capacity of air reaches 385.4 W and the COP reaches 2.84. When the inlet air velocity is 1 m/s, the average cooling capacity of air reaches 159.1 W and the COP reaches 1.17. When the inlet air humidity is 50%, the average cooling capacity of air reaches 366.7 W and the COP reaches 2.69. An efficient DCHE requires the reduction of hot water temperature and the mitigation of both inlet air humidity and velocity, thereby enhancing regeneration efficiency through minimizing the system's energy demands.

Data availability

The data that support the findings of this study are available from the corresponding author upon reasonable request.

Received: 7 October 2024; Accepted: 10 February 2025
Published online: 03 March 2025

References

1. Tu, Y. D., Wang, R. Z., Ge, T. S. & Zheng, X. Comfortable, high-efficiency heat pump with desiccant-coated, water-sorbing heat exchangers. *Sci. Rep.* **7**(1). (2017).
2. Qu, M., Abdelaziz, O., Gao, Z. & Yin, H. Isothermal membrane-based air dehumidification: A comprehensive review. *Renew. Sustain. Energy Rev.* **82**, 4060–4069 (2018).
3. Liu, X. et al. Power generation from ambient humidity using protein nanowires. *Nature* **578** (7796), 550–554 (2020).
4. Yu, Z. et al. Interfacial solar evaporator for clean water production and beyond: from design to application. *Appl. Energy* ;**299**. (2021).
5. Zhao, J., Tu, Z. & Chan, S. H. In-situ measurement of humidity distribution and its effect on the performance of a proton exchange membrane fuel cell. *Energy* ;**239**. (2022).
6. Huang, H., Wang, H., Hu, Y-J., Li, C. & Wang, X. Optimal plan for energy conservation and CO2 emissions reduction of public buildings considering users' behavior: Case of China. *Energy* ;261. (2022).
7. Zhao, L. H., Wang, R. Z. & Ge, T. S. Desiccant coated heat exchanger and its applications. *Int. J. Refrig.* **130**, 217–232 (2021).
8. Dai, Y. et al. Hybrid liquid desiccant air-conditioning system combined with marine aerosol removal driven by low-temperature heat source. *Appl. Energy* ;**275**. (2020).
9. Cui, S. et al. Metal-Organic frameworks as advanced moisture sorbents for energy-efficient high temperature cooling. *Sci. Rep.* ;**8**(1). (2018).
10. Gorai, V. K., Singh, S. K. & Jani, D. B. A comprehensive review on solid desiccant-assisted novel dehumidification and its advanced regeneration methods. *J. Therm. Anal. Calorim.* **149** (17), 8979–9000 (2024).
11. Daou, K., Wang, R. & Xia, Z. Desiccant cooling air conditioning: A review. *Renew. Sustain. Energy Rev.* **10** (2), 55–77 (2006).
12. Ge, T. S., Dai, Y. J., Wang, R. Z. & Peng, Z. Z. Experimental comparison and analysis on silica gel and polymer coated fin-tube heat exchangers. *Energy* **35** (7), 2893–2900 (2010).
13. Jani, D. B., Mishra, M. & Sahoo, P. K. Solid desiccant air conditioning – a state of the art review. *Renew. Sustain. Energy Rev.* **60**, 1451–1469 (2016).
14. Kim, H. et al. Water harvesting from air with metal-organic frameworks powered by natural sunlight. *Science* **356** (6336), 430–434 (2017).
15. Karmakar, A., Prabakaran, V., Zhao, D. & Chua, K. J. A review of metal-organic frameworks (MOFs) as energy-efficient desiccants for adsorption driven heat-transformation applications. *Appl. Energy* ;**269**. (2020).
16. Hanikel, N. et al. Evolution of water structures in metal-organic frameworks for improved atmospheric water harvesting. *Science* **374** (6566), 454–459 (2021).
17. Bezrukov, A. A. et al. Metal-organic frameworks as regeneration optimized sorbents for atmospheric water harvesting. *Cell. Rep. Phys. Sci.* ;**4**(2). (2023).
18. Gordeeva, L. G. et al. Metal-organic frameworks for energy conversion and water harvesting: A bridge between thermal engineering and material science. *Nano Energy* ;**84**. (2021).
19. Feng, Y., Ge, T., Chen, B., Zhan, G. & Wang, R. A regulation strategy of sorbent stepwise position for boosting atmospheric water harvesting in arid area. *Cell. Rep. Phys. Sci.* ;**2**(9). (2021).
20. Amani, M. & Bahrami, M. Greenhouse dehumidification by zeolite-based desiccant coated heat exchanger. *Appl. Therm. Eng.* ;**183**. (2021).
21. LaPotin, A. et al. Dual-stage atmospheric water harvesting device for scalable solar-driven water production. *Joule* **5** (1), 166–182 (2021).
22. Meng, Y., Dang, Y. & Suib, S. L. Materials and devices for atmospheric water harvesting. *Cell. Rep. Phys. Sci.* ;**3**(7). (2022).

23. Ge, T. S., Dai, Y. J. & Wang, R. Z. Analysis on integrated low grade condensation heat powered desiccant coated vapor compression system. *Appl. Therm. Eng.* **138**, 307–318 (2018).
24. Gentile, V., Bozlar, M., Meggers, F. & Simonetti, M. Liter-scale atmospheric water harvesting for dry climates driven by low temperature solar heat. *Energy* ;**254**. (2022).
25. Entezari, A., Ejeian, M. & Wang, R. Modifying water sorption properties with polymer additives for atmospheric water harvesting applications. *Appl. Therm. Eng.* ;**161**. (2019).
26. Zheng, X., Ge, T. S., Jiang, Y. & Wang, R. Z. Experimental study on silica gel-LiCl composite desiccants for desiccant coated heat exchanger. *Int. J. Refrig.* **51**, 24–32 (2015).
27. Fang, Y. et al. Preparation and performance of desiccant coating with modified ion exchange resin on finned tube heat exchanger. *Appl. Therm. Eng.* **93**, 36–42 (2016).
28. Chung, J. Y. et al. Comparative performance evaluation of multi-objective optimized desiccant wheels coated with MIL-100 (fe) and silica gel composite. *Energy* ;**283**. (2023).
29. Bai, Z. et al. Performance evaluation of PVA/PEO/LiCl composite as coated heat exchangers desiccants. *Int. J. Refrig.* **154**, 258–267 (2023).
30. Mittal, H., Alili, A. A. & Alhassan, S. M. Hybrid super-porous hydrogel composites with high water vapor adsorption capacity – adsorption isotherm and kinetics studies. *J. Environ. Chem. Eng.* ;**9**(6). (2021).
31. Pan, Y. et al. An ultra-hygroscopic polymer for high-efficiency dehumidification. *Cell. Rep. Phys. Sci.* ;**4**(9). (2023).
32. Pan, Q. W. et al. Performance assessment of heat exchanger coated with encapsulated ultra-high salt content desiccant. *Appl. Therm. Eng.* ;231. (2023).
33. Zheng, X., Zhang, Y., Wan, T. & Chen, K. Experimental study on the performance of a novel superabsorbent polymer and activated carbon composite coated heat exchangers. *Energy* ;**281**. (2023).
34. Chen, W. D., Vivekh, P., Liu, M. Z., Kumja, M. & Chua, K. J. Energy improvement and performance prediction of desiccant coated dehumidifiers based on dimensional and scaling analysis. *Appl. Energy* ;**303**. (2021).
35. Zu, K. & Qin, M. Optimization of the hygrothermal performance of novel metal-organic framework (MOF) based humidity pump: A CFD approach. *Energy* ;**259**. (2022).
36. Jagirdar, M. & Lee, P. S. Mathematical modeling and performance evaluation of a desiccant coated fin-tube heat exchanger. *Appl. Energy*. **212**, 401–415 (2018).
37. Zanoni, M. A. B., Wang, J., Torero, J. L. & Gerhard, J. I. Multiphase modelling of water evaporation and condensation in an air-heated porous medium. *Appl. Therm. Eng.* ;**212**. (2022).
38. Khatibi, M., Mohammadzadeh Kowsari, M., Golparvar, B. & Niazmand, H. Optimum loading of aluminum additive particles in unconsolidated beds of finned flat-tube heat exchangers in an adsorption cooling system. *Appl. Therm. Eng.* ;**196**. (2021).
39. Keramati, H., Hamdullahpur, F. & Barzegari, M. Deep reinforcement learning for heat exchanger shape optimization. *Int. J. Heat Mass Transf.* ;**194**. (2022).
40. Agrawal, A., Kumar, A. & Parekh, A. D. Experimental investigation of solar driven atmospheric water generation system based on air-to-air heat exchanger. *Energy* ;**271**. (2023).

Acknowledgements

This research work is funded by the General projects of the National Foundation of China 52376203.

Author contributions

Xiaoping Lei(first author): Formal Analysis, Writing - Original Draft、Visualization.Wenjun Ying: Resources, Software.Zhaoran Xue: Investigation, Data Curation.Hua Zhang: Conceptualization, Supervision.Jiayun Wang: Methodology，Reviewing and Editing the final manuscript.All authors reviewed the manuscript.

Declarations

Competing interests

The authors declare no competing interests.

Additional information

Correspondence and requests for materials should be addressed to J.W.

Reprints and permissions information is available at www.nature.com/reprints.

Publisher's note Springer Nature remains neutral with regard to jurisdictional claims in published maps and institutional affiliations.